Heat Mass Transfer (2007) 43: 233–241
DOI 10.1007/s00231-006-0090-1

ORIGINAL

K. Krabbenhoft · L. Damkilde · M. Nazem

An implicit mixed enthalpy–temperature method for phase-change problems

Received: 11 January 2005 / Accepted: 9 January 2006 / Published online: 11 March 2006

Abstract A finite element procedure for phase-change problems is presented. Enthalpy and temperature are interpolated separately and subsequently linked via the appropriate relation in the nodes of the mesh during the solution phase. A novel technique is here used where, depending on the characteristics of the problem, either temperature or enthalpy may be considered as primary variable. The resulting algorithm is both efficient and robust and is further easy to implement and generalize to arbitrary finite elements. The capabilities of the method are illustrated by the solution both isothermal and non-isothermal phase-change problems.

1 Introduction

In a large number of problems of engineering interest, the transition of the material from one phase to another is of vital importance in describing the overall physical behaviour. Common applications include metal casting, freezing and thawing of foodstuffs and other biological materials, ground freezing and solar energy storage.

The phase-change problem is characterized by an abrupt change in enthalpy per unit temperature in a narrow temperature range around the freezing point. Indeed, it is often assumed that the enthalpy increases by some, usually rather large, amount at one characteristic temperature as shown in Fig. 1a. This assumption gives rise to a moving boundary problem which in quite a few cases can be solved analytically or otherwise by approximate hand calculation methods, see [1, 2].

K. Krabbenhoft (✉) · M. Nazem
Civil, Surveying and Environmental Engineering,
University of Newcastle, NSW, Newcastle, Australia
E-mail: kristian.krabbenhoft@newcastle.edu.au

L. Damkilde
Department of Engineering, Aalborg University,
Esbjerg, Denmark

For many real problems such as the ones listed in the above, the change of phase does not take place at one characteristic temperature but over a temperature range as shown in Fig. 1b. One speaks of a mushy zone where at a given temperature both fluid and solid material may exist. This problem is no longer a moving boundary problem but rather a non-linear diffusion problem.

Usually, the mushy zone is sufficiently narrow for the assumption of isothermal phase-change to be a good approximation. However, whereas the isothermal phase-change assumption is convenient as a means at arriving at closed-form analytical solutions it can cause significant complications when it comes to numerical solution methods. To address the problem of a moving front explicitly so-called front-tracking methods have been devised. As the name suggests these methods track the solid–liquid interface and attempt at fulfilling the boundary conditions associated with the moving interface. The front-tracking methods usually involve a continuously deforming mesh which in itself is a considerable complication. Other complications include the treatment of multiple interfaces, appearing and disappearing fronts, and of course the inability to deal with non-isothermal phase-change problems. For these reasons the front-tracking methods have been applied mostly to simple one dimensional problems, although limited attempts at generalization to two spatial dimensions have also been carried out, see e.g. [3].

The alternative to the front-tracking methods are the fixed grid methods. These methods solve the weak form of the governing equations on a fixed grid without making any explicit reference to the conditions on the moving interface. For this reason they are also sometimes referred to as front-capturing methods. The fixed grid methods are more general than the front-tracking methods in that both isothermal and non-isothermal phase-change can be handled. Moreover, most fixed grid methods are not too difficult to extend from one to two and three spatial dimensions. The various fixed grid methods may again be subdivided into different categories depending on how the latent heat is accounted

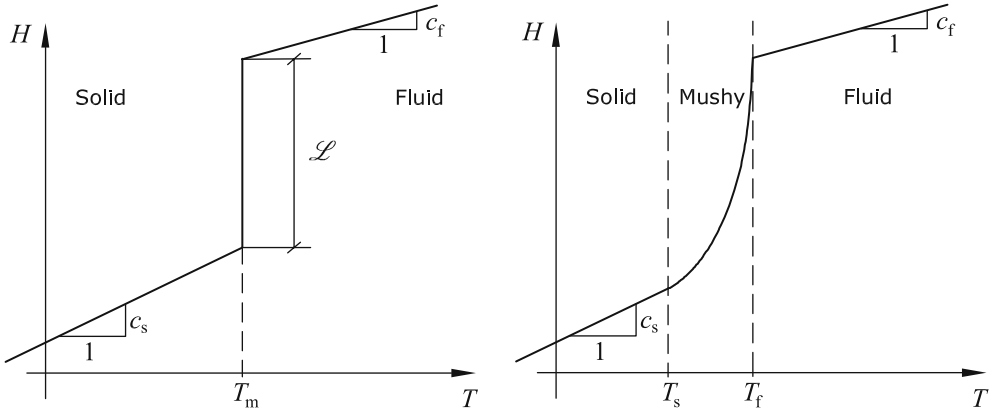

Fig. 1 Enthalpy–temperature relations for isothermal (**a**) and non-isothermal phase change (**b**)

for. Two broad classes can here be identified: effective heat capacity methods and source methods.

The main challenge in the application of the effective heat capacity methods is that a heat capacity around the melting varies very rapidly and may be missed altogether if special procedures are not used. Therefore, some representative average quantity is usually used and large number of averaging schemes can be found in the literature, a review of which is given in Lewis et al. [4].

With the source methods the sensible and latent heats are separated and each quantity discretized in space using standard finite elements. This yields a set of non-linear equations which must be solved iteratively. If the standard Newton–Raphson procedure is used the Jacobian is needed. It turns out that the part of the Jacobian associated with the latent heat is crucial for the convergence of the iterations. In the case of isothermal phase-change the latent heat vector is evaluated exactly, i.e. by splitting up the domain into a solid and a liquid fraction and then integrating over each domain. If this is done, the exact Jacobian can be derived analytically as shown by Storti et al. [5]. Generally speaking, this is of course an attractive feature. However, only in the case of isothermal phase-change and for simple elements such as the linear triangle is the integration of latent heat contribution and its associated Jacobian straightforward (see e.g. [6] for the implementation in the plane isoparametric four-node element). In the case of non-isothermal phase-change the implementation becomes even more demanding with the elements being split up in solid, liquid and mushy regions, see [7, 8]. Moreover, because of the 'consistent' evaluation of the latent heat, temperature oscillations may occur as shown in [7]. As in linear heat conduction with a consistent capacitance matrix the only cure for this problem is for a given time step to refine the mesh or alternatively, for a given mesh to increase the time step. Thus, the full potential of a given spatial discretization cannot be realized because the time step must be adjusted accordingly.

In the following a new implicit method capable of dealing with generalized phase-change problems is presented. The procedure does not require a division of the domain into liquid and solid part and is in this sense similar to the effective heat capacity methods. However, the resulting equations are solved iteratively (to within a specified tolerance) as with the source methods. Both the enthalpy and the temperature are discretized separately and then subsequently linked in the nodes of the finite element mesh during the iterative solution procedure. This iterative procedure differs from the standard Newton–Raphson scheme in that a modified update rule is used. This rule effectively avoids the drawbacks of temperature based formulations while at the same time formally retaining the temperature as the primary variable.

2 Governing equations

We consider the heat conduction equation [7]

$$\frac{\partial H}{\partial t} - \nabla \cdot (k \nabla T) = Q, \quad \mathbf{x} \in \Omega,\ t \in \Upsilon = [0, \tau], \tag{1}$$

where H it the enthalpy, T the temperature, k the conductivity and Q an internal heat source/sink. The governing Eq. 1 is supplemented with the initial condition

$$T(\mathbf{x}, t = 0) = T_0(\mathbf{x}) \quad \text{in } \Omega \tag{2}$$

and the boundary conditions

$$\begin{aligned} T &= T_b && \text{on } \partial\Omega_T \times \Upsilon, \\ (k\nabla T) \cdot \mathbf{n} &= q && \text{on } \partial\Omega_q \times \Upsilon, \\ (k\nabla T) \cdot \mathbf{n} &= \beta(T_\infty - T) && \text{on } \partial\Omega_c \times \Upsilon, \end{aligned} \tag{3}$$

where $\partial\Omega_{\mathrm{T}}$, $\partial\Omega_{\mathrm{q}}$, and $\partial\Omega_{\mathrm{c}}$ are non-overlapping portions of the boundary of Ω, T and q are the specified temperature and flux at $\partial\Omega_{\mathrm{T}}$ and $\partial\Omega_{\mathrm{q}}$, respectively, β is the heat convection coefficient and T_∞ the environment temperature.

In order to solve Eqs. 1, 2 and 3 a relation between temperature and enthalpy must be established. Instead of aiming at a closed-form expression for the enthalpy–temperature relation it is more convenient to consider the liquid fraction u_ℓ as a function of temperature. That is, when the temperature of a certain medium, e.g. a

metallic alloy, is lowered from some point above the freezing point T_f, Fig. 1b, the liquid fraction contained within the medium will gradually decrease until all liquid has undergone change of phase. The enthalpy can then be defined as

$$H = \int_{T_{\text{ref}}}^{T} \rho c(T)\,\mathrm{d}T + \rho \mathscr{L} u_\ell = H^{\text{S}} + H^{\text{L}}, \tag{4}$$

where $\mathscr{L}$ is the latent heat and $c(T)$ is the specific heat. Thus, the total enthalpy may be partitioned into two contributions, sensible heat H^{S} and latent heat H^{L}. In the important special case where the sensible heat is a linear function of the temperature, but with different specific heats c_f and c_s in the liquid and solid states, the total enthalpy can be written as

$$H = [\rho c_f u_\ell + \rho c_s(1-u_\ell)](T - T_f) + \rho \mathscr{L} u_\ell, \tag{5}$$

which, if u_ℓ is smooth, yields a smooth total enthalpy–temperature relation.

3 Discretization

In the following the temporal and spatial discretizations of Eqs. 1, 2 and 3 are briefly described.

3.1 Spatial discretization

Both the temperature and the enthalpy variables are approximated by finite element functions, i.e.

$$T(\mathbf{x},t) \approx \mathbf{N}(\mathbf{x})\mathbf{T}(t), \quad H(\mathbf{x},t) \approx \mathbf{N}(\mathbf{x})\mathbf{H}(t). \tag{6}$$

This leads to a set of ordinary differential equations given by

$$\mathbf{r} = \mathbf{M}\frac{\mathrm{d}\mathbf{H}}{\mathrm{d}t} + \mathbf{K}\mathbf{T} - \mathbf{f} = \mathbf{0}, \tag{7}$$

where

$$\begin{aligned}
\mathbf{M} &= \int_\Omega \mathbf{N}^T\mathbf{N}\,\mathrm{d}\Omega,\\
\mathbf{K} &= \int_\Omega \mathbf{B}^T k\,\mathbf{B}\,\mathrm{d}\Omega + \int_{\partial\Omega_c} \mathbf{N}^T h \mathbf{N}\,\mathrm{d}\Gamma,\\
\mathbf{f} &= \int_\Omega \mathbf{N}^T Q\,\mathrm{d}\Omega + \int_{\partial\Omega_q} \mathbf{N}^T q\,\mathrm{d}\Gamma + \int_{\partial\Omega_c} \mathbf{N}^T h T_\infty\,\mathrm{d}\Gamma.
\end{aligned} \tag{8}$$

Note that in practice $\mathbf{M}$ is often lumped. For the low-order elements used here this lumping is straightforward and will be implicitly assumed in the following. Thus, for an element defined by n_{dof} nodes we have

$$\mathbf{M} = \frac{V}{n_{\text{dof}}}\mathbf{I}, \tag{9}$$

where V is the element area and $\mathbf{I}$ the unit matrix.

3.2 Temporal discretization

Two different methods of time discretization have been considered. The first is the basic backward Euler scheme by which Eq. 7 is approximated as

$$\mathbf{r}_{n+1} = \mathbf{M}\mathbf{T}_{n+1} - \mathbf{M}\mathbf{T}_n + \Delta t \mathbf{K}_{n+1}\mathbf{T}_{n+1} - \Delta t \mathbf{f}_{n+1} = \mathbf{0}. \tag{10}$$

Secondly, we consider the following approximation of the time derivative

$$\frac{\mathrm{d}\mathbf{H}}{\mathrm{d}t} \approx \frac{3\mathbf{H}_{n+1} - 4\mathbf{H}_n + \mathbf{H}_{n-1}}{2\Delta t}. \tag{11}$$

So that the final discrete system is given by

$$\begin{aligned}
\mathbf{r}_{n+1} &= \mathbf{M}(3\mathbf{H}_{n+1} - 4\mathbf{H}_n + \mathbf{H}_{n-1}) + \Delta t \mathbf{K}_{n+1}\mathbf{T}_{n+1} - \Delta t \mathbf{f}_{n+1}\\
&= \mathbf{0}.
\end{aligned} \tag{12}$$

The approximation (11), which has second order accuracy, has previously been applied to the Richards equation describing flow of water in unsaturated soils by Celia et al. [9]. Some gains were reported and since the problem studied here in many ways is similar to the unsaturated flow problem, similar gains may be expected. Examples demonstrating the effects of the above temporal discretization will be given in Section 5. It should be mentioned that we have also implemented the Adams–Moulton approximation

$$\frac{\mathrm{d}\mathbf{H}}{\mathrm{d}t} \approx \frac{\mathbf{H}_{n+1} - \mathbf{H}_{n-1}}{2\Delta t}, \tag{13}$$

which also posses second order accuracy. However, in practice the results have been quite discouraging, i.e. regarding accuracy the approximation is not much better than the standard Euler scheme and often even worse. Furthermore, the non–physical oscillations are generally much more pronounced than with the use of (11). For these reasons the Adams–Moulton approximation will not be treated any further.

3.3 Tangent matrices

The iterative procedure presented in the next section requires the Jacobian (tangent matrix) of the residuals given in Eqs. 10 and 12. In the following the tangent matrix associated with the conductivity matrix is treated in some detail.

For the integration of matrix, two different approaches may be applied. In the first, the integration is performed as

$$\mathbf{K} = \int_\Omega \mathbf{B}^T k\,(\mathbf{A}\mathbf{T})\mathbf{B}\,\mathrm{d}\Omega, \tag{14}$$

where $\mathbf{A}$ is an appropriately chosen set of shape functions determining the distribution of the conductivity over an element. Here it could be argued that $\mathbf{A} = \mathbf{N}$ is the natural choice. The tangent matrix associated with $\mathbf{K}$ is given by

$$\mathbf{K}_t = \frac{\partial^T}{\partial \mathbf{T}}(\mathbf{K}\mathbf{T}) = \mathbf{K} + \int_\Omega \mathbf{B}^T k'(\mathbf{A}\mathbf{T})\mathbf{B}\mathbf{T}\mathbf{A}\,\mathrm{d}\Omega a, \tag{15}$$

where $k' = \mathrm{d}k/\mathrm{d}T$. If numerical integration is used the same scheme should be used throughout. As can be seen, $\mathbf{K}_t$ consists of the original symmetric conductivity matrix and a non-symmetric contribution.

In the second approach to the integration of $\mathbf{K}$ the conductivity k is interpolated in a similar way as the enthalpy and temperature variables, i.e.

$$k(T) \approx \mathbf{A}\mathbf{k} \tag{16}$$

where $\mathbf{k} = [k(T_1), \ldots, k(T_{n_{\mathrm{dof}}})]^T$, contains the nodal conductivities. In this way $\mathbf{K}$ is given by

$$\mathbf{K} = \int_\Omega \mathbf{B}^T\mathbf{A}\mathbf{k}\mathbf{B}\,\mathrm{d}\Omega \tag{17}$$

and the associated tangent matrix is

$$\mathbf{K}_t = \frac{\partial^T}{\partial \mathbf{T}}(\mathbf{K}\mathbf{T}) = \mathbf{K} + \left[\int_\Omega \mathbf{B}^T\mathbf{A}\mathbf{k}\mathbf{B}\mathbf{T}\mathbf{A}\,\mathrm{d}\Omega\right]\mathrm{diag}(\mathbf{k}'), \tag{18}$$

where $\mathbf{k}' = [k'(T_1), \ldots, k'(T_{n_{\mathrm{dof}}})]^T$.

An efficient special case consists of taking $\mathbf{A}$ as being constant, for example with all entries equal to $1/n_{\mathrm{dof}}$. We can then define

$$\tilde{\mathbf{K}} = \int_\Omega \mathbf{B}^T\mathbf{B}\,\mathrm{d}\Omega \tag{19}$$

and subsequently compute $\mathbf{K}$ as

$$\mathbf{K} = \tilde{\mathbf{K}}\mathbf{A}\mathbf{k} \tag{20}$$

and $\mathbf{K}_t$ as

$$\mathbf{K} = \mathbf{K} + \tilde{\mathbf{K}}\mathbf{A}\mathbf{k}\mathrm{diag}(\mathbf{k}'). \tag{21}$$

The full Jacobian can now be written as

$$\mathbf{J} = \frac{\partial^T \mathbf{r}}{\partial \mathbf{T}} = \mathbf{M}\mathbf{G} + \Delta t\,\mathbf{K}_t, \tag{22}$$

where $\mathbf{G}$ is a diagonal matrix containing the derivative of the enthalpy–temperature relation evaluated at the nodes of the mesh:

$$G = \begin{bmatrix} (\mathrm{d}H/\mathrm{d}T)_1 & & \\ & \ddots & \\ & & (\mathrm{d}H/\mathrm{d}T)_{n_{\mathrm{dof}}} \end{bmatrix}. \tag{23}$$

4 Solution algorithm

The discrete equations 10 now contain both the nodal enthalpies and the nodal temperatures and a choice must be made as to which of these should be used as primary variable in the iterative solution procedure. Since enthalpy is usually given in terms of temperature and not vice versa it seems natural to use the temperature as primary variable. The Newton–Raphson scheme can then be written as

$$\begin{aligned} \Delta\mathbf{T}^j_{n+1} &= -(\mathbf{J}^j_{n+1})^{-1}\mathbf{r}^j_{n+1}, \\ \mathbf{T}^{j+1}_{n+1} &= \mathbf{T}^j_{n+1} + \Delta\mathbf{T}^j_{n+1}, \\ \mathbf{H}^{j+1}_{n+1} &= H(\mathbf{T}^{j+1}_{n+1}). \end{aligned} \tag{24}$$

In each iteration, temperature increments $\mathbf{T}$ are computed and the temperatures then updated. On the basis of these temperatures the corresponding enthalpies are computed by means of the relevant enthalpy–temperature relation.

This series of steps is in some sense consistent with the Newton–Raphson method, but is by no means the only way to proceed. The problem with the procedure is that if the enthalpy–temperature curve is very steep around the phase-change temperature, then the chances of producing pairs (T,H) lying in the narrow mushy zone is very slight, and the large gradients associated with such points will be missed in the tangent matrix. This may slow down convergence or, in most cases in fact, lead to situations where convergence is not achieved unless line search or other similar procedures are used.

One way of countering these problems is to, instead of computing the nodal enthalpies on the basis of the nodal temperatures, compute some enthalpy increment $\mathbf{H}$ on the basis of the temperature increment, then update the nodal enthalpies and finally, compute the temperatures corresponding to these enthalpies. Thus, the iterative procedure can be written principally as

$$\begin{aligned} \Delta\mathbf{T}^j_{n+1} &= -(\mathbf{J}^j_{n+1})^{-1}\mathbf{r}^j_{n+1}, \\ \Delta\mathbf{H}^j_{n+1} &= G(\Delta\mathbf{T}^j_{n+1}), \\ \mathbf{H}^{j+1}_{n+1} &= \mathbf{H}^j_{n+1} + \Delta\mathbf{H}^j_{n+1}, \\ \mathbf{T}^{j+1}_{n+1} &= T(\mathbf{H}^{j+1}_{n+1}). \end{aligned} \tag{25}$$

The question is now how the enthalpy increments should be computed. Here is seems natural to use the Taylor expansion

$$\mathbf{H} = \mathbf{H}^j_{n+1} + \left(\frac{\mathrm{d}\mathbf{H}}{\mathrm{d}\mathbf{T}}\right)^j_{n+1}\Delta\mathbf{T}^j_{n+1} \tag{26}$$

and thus,

$$\Delta\mathbf{H}^j_{n+1} = \mathbf{G}^j_{n+1}\Delta\mathbf{T}^j_{n+1}, \tag{27}$$

where

$$\mathbf{G}^j_{n+1} = \left(\frac{\mathrm{d}\mathbf{H}}{\mathrm{d}\mathbf{T}}\right)^j_{n+1}. \tag{28}$$

The difference between the two different types of temperature and enthalpy update is illustrated in Fig. 2

a. From an equilibrium point A a temperature increment is computed. If the conventional update is used an intermediate point A' is found after which the enthalpy–temperature relation is used to bring the solution to point A''. In this case the mushy zone is missed which may result in the problems described in the above.

If the alternative method of update is used we are again initially at point A. On the basis of the temperature increment ΔT an enthalpy increment is computed to bring the solution to the intermediate point B from which the inverse enthalpy–temperature relation is used to finally arrive at point B'. In the next iteration the tangent matrix will now reflect the fact that the node is undergoing change of phase and chances of convergence should be much better.

However, the alternative method of update is not completely without any complications and generally, care should be taken when computing enthalpy increments. This is illustrated in Fig. 2 (b), where the initial point lies in the mushy zone. Since $\mathrm{d}H/\mathrm{d}T$ is now large, the temperature increment will generally be quite small. However, since the gradient is large, even small increments will result in large changes. Again, the two different methods of update are considered. The conventional method produces points A–A'–A'' and thus, the overall change is moderate. The alternative update, however, results in a rather large change in enthalpy, A–B, which results in an even larger change in temperature, B–B'. Thus, the difference between the points produced by the two different methods is quite pronounced and which point is closer to the real solution of course depends on the particular circumstances. It can, however, be seen that the alternative update, just as the conventional one, may produce large increments under circumstances which may require more moderate changes.

Thus, it seems that the optimal method of update should embrace a combination of these two different methods of update. Alternatively, depending on the particular state, each node may be updated by either of the two methods. The critical issue is then the formulation of a proper test to decide as to which of the two methods of update should be applied for a given node. With these considerations in mind, a simple approach would be to choose the update which gives the smallest temperature increment. Thus, the algorithm used in the following can be summarized by

$$
\begin{aligned}
&\Delta\mathbf{T}_A = -(\mathbf{J}^j_{n+1})^{-1}\mathbf{r}^j_{n+1},\\
&\Delta\mathbf{T}_B = T(\mathbf{H}^j_{n+1} + \mathbf{G}^j_{n+1}\Delta\mathbf{T}_A) - \mathbf{T}^j_{n+1},\\
&\quad k = 1,\ldots,\text{No nodes}\\
&\qquad \text{if } \left|\Delta T^k_A\right| < \left|\Delta T^k_B\right| \qquad (29)\\
&\qquad \text{then } \Delta T^k = \Delta T^k_A\\
&\qquad \text{else } \Delta T^k = \Delta T^k_B\\
&\mathbf{T}^{j+1}_{n+1} = \mathbf{T}^j_{n+1} + \Delta\mathbf{T}^j_{n+1}.
\end{aligned}
$$

Of course, other criteria for selecting the type of update may be used. The strategy used in the above may not be the most efficient in the sense that it is overly cautious. On the other hand, this makes the iterative procedure very robust and furthermore, no special parameters are needed to decide on the choice of update type.

The procedure presented above has some similarities with the method of Nedjar [10]. Here the enthalpy was used as the primary variable and the temperatures then updated based on the enthalpy. In the present procedure, however, temperature is retained as the primary variable in the 'global' heat balance equations 10. On the 'local' level, when updating the temperature at each

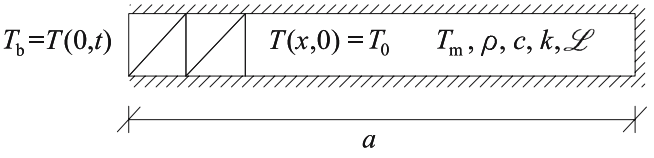

Fig. 3 Configuration of Example 1

Table 1 Parameters used in Example 1

$a = 4.0$ m	$\rho = 1.0$ kg/m^3
$T_0 = 0.0$°C	$c = 1.0$ J/(Kkg)
$T_b = -45.0$°C	$k = 1.08$ W/(K,m)
$T_m = -0.1$°C	$\mathscr{L} = 70.26$ J/kg

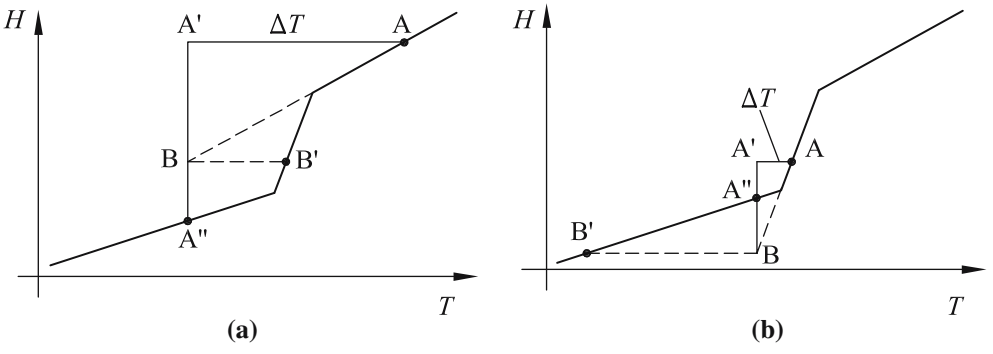

Fig. 2 Iterative procedure

node, a procedure which is equivalent to a change of variable is performed if the circumstances for doing so are deemed favorable. Thus, the method combines the use of temperature and enthalpy as primary variables and should therefore in a certain sense, at least with the right criterion for choosing the type of update, be optimal.

For the examples presented in Section 5, the iterations are broken off when the following criteria are satisfied

$$\left\|\mathbf{r}_{n+1}^{j+1}\right\| < \varepsilon_1 \max\left(1, \left\|\mathbf{MH}_{n+1}^{j+1}\right\|\right) \tag{30}$$

and

$$\left\|\Delta\mathbf{T}_{n+1}^{j}\right\| < \varepsilon_2 \max\left(1, \left\|\mathbf{T}_{n+1}^{j+1} - \mathbf{T}_n\right\|\right) \tag{31}$$

In the following we use $\varepsilon_1 = \varepsilon_2 = 10^{-9}$.

5 Examples

In the following three examples demonstrating the capabilities of the proposed method are given.

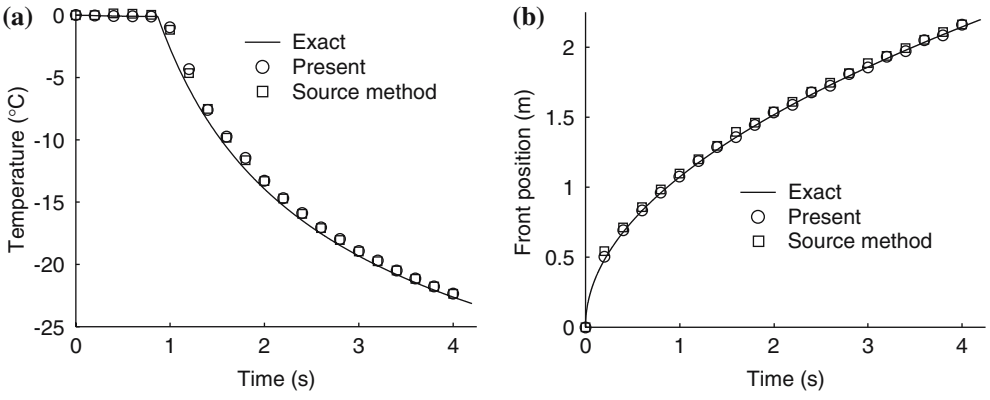

Fig. 4 Example 1, $h = 0.125$ m, D $t = 0.2$ s. Temperature at $x = 1.0$ m (**a**) and front position (**b**)

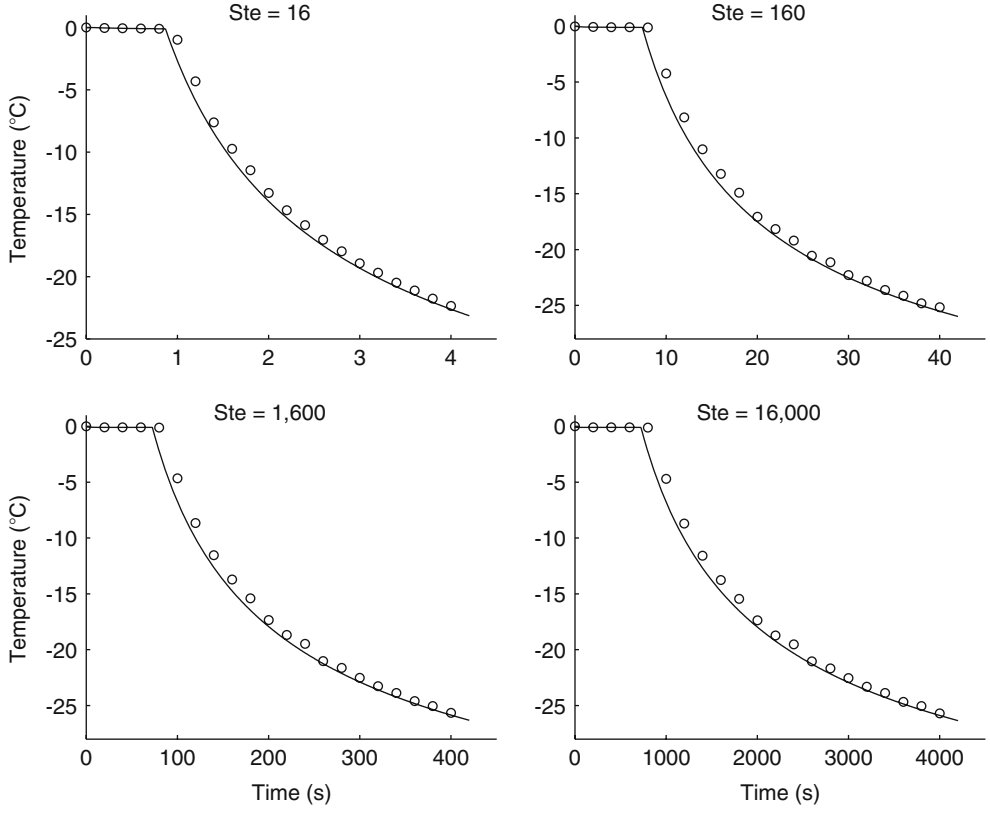

Fig. 5 Example 1. Temperature at $x = 1.0$ m for different Stefan numbers

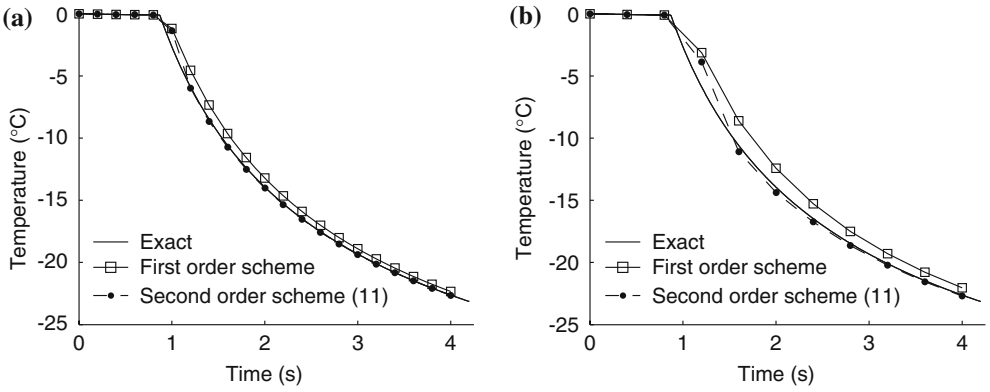

Fig. 6 Example 1. Effect of higher order temporal discretization $h = a/256$ m. Temperature at $x = 1.0$ m for D $t = 0.2$ s (**a**) and for D $t = 0.4$ s (**b**)

5.1 Example 1: one-dimensional solidification

A standard test example for isothermal phase-change, see e.g. [4–8], considers the solidification of a one-dimensional slab as shown in Fig. 3. The analytical solution for a semi–infinite slab can be found in [1, 2]. The problem is defined by the material parameters and initial and boundary conditions given in Table 1. As in [7] we use 2×32 triangular elements positioned as indicated in Fig. 3, i.e. the mesh size is $h = 0.125$ m. The time step is $\Delta t = 0.2$ s and the liquid fraction is approximated by a straight line from $T_f = T_m = -0.1$°C to $T_s = -0.1001$°C i.e. the mushy zone has an extent of 10^{-4}°C. The material parameters given in Table 1 define a Stefan number of

$$\mathrm{St} = \frac{\rho \mathscr{L}}{\rho c (T_m - T_b)} = 1.6. \tag{32}$$

In Figure 4 the temperature evolution at 1.0 m is shown together with the front position. As can be seen the results produced by the two methods are hardly distinguishable. For the present method the problem poses no particular difficulties, the average number of iterations being only 2.9 on average. As for the source method we found, in accordance with [11], that a line search was necessary in order to achieve convergence in the first few time steps.

Next, four runs with Stefan numbers equal to St = 16, 160, 1,600 and 160,000 are performed. These problems were generated by increasing the latent heat whereas all other material, boundary and mesh data remain unchanged. The time steps were chosen as $\Delta t = 2$, 20, 200, 2,000 s, respectively. The results of these analyses are shown in Fig. 5. As can be seen there is virtually no difference in the quality of the solutions.

Finally, to test the second order accurate temporal discretization 31 we run the same example with $h = a/256$ m and $\Delta t = 0.2$ and 0.4s, respectively. The results are shown in Fig. 6 and suggest that the second order accurate discretization may be rather efficient. It should be borne in mind, however, that the higher order approximation does not posses the same good stability properties as the standard backward Euler scheme, and may result in non–physical temperature oscillations although for a wide range of realistic examples these have generally been found to be very moderate.

5.2 Example 2: two-dimensional solidification

The next example concerns the solidification corner region as shown in Fig. 7. An analytical solution to this problem has been given by Rathjen and Jiji [11]. The

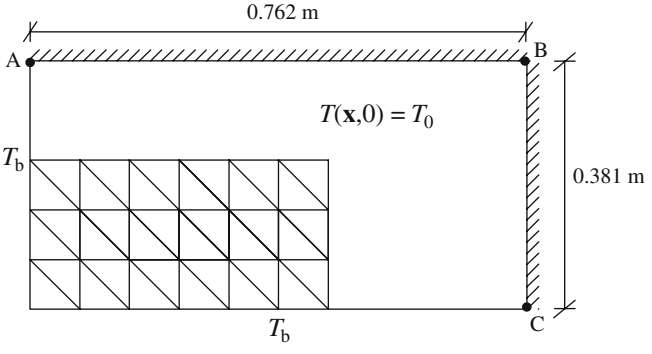

Fig. 7 Configuration of Example 2

Table 2 Parameters used in Example 2

$T_0 = 1{,}550$°C	$\rho\, c = 5.4 \times 10^6$ J/(Km^3)
$T_b = 1{,}150$°C	$k = 30$ W/(Km)
$T_m = 1{,}500$°C	$\rho \mathscr{L} = 1.89 \times 10^9$ J/m^3

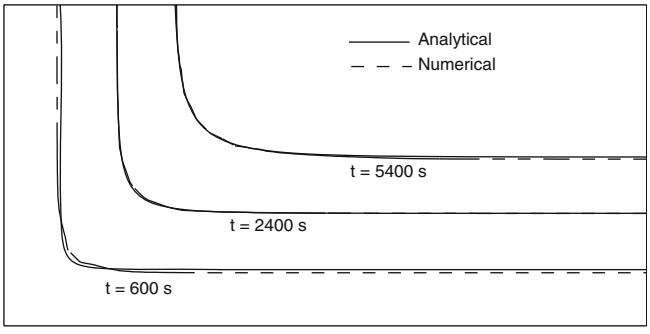

Fig. 8 Example 2. Front positions at different times

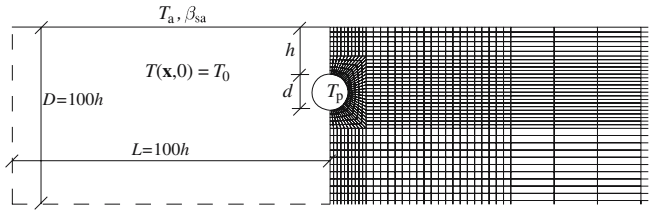

Fig. 9 Configuration of Example 3 (coarse mesh)

Table 3 Parameters used in Example 2

$\rho = 1{,}000\ \text{kg/m}^3$	$\rho_s = 2{,}200\ \text{kg/m}^3$
$c_w = 4{,}200\ \text{J/Kkg}$	$k_w = 0.56\ \text{W/mK}$
$c_i = 1{,}760\ \text{J/Kkg}$	$k_i = 2.2\ \text{W/mK}$
$c_s = 780\ \text{J/Kkg}$	$k_s = 1.4\ \text{W/mK}$
$\mathscr{L} = 338{,}000\ \text{J/kg}$	$n = 0.3$
$\beta_{sa} = 10.0$	$T_m = 0.0°\text{C}$
$T_a = -°\text{C}$	$T_0 = 2.0°\text{C}$
$T_p = 1.0°\text{C}$	$a = -1.19°\text{C}$
$b = 1.6$	$h = 1.5\ \text{m}$
$a = 1.0\ \text{m}$	$W_0 = 0.04$

material parameters and initial and boundary conditions are given in Table 2. A regular 25×50 mesh constructed as indicated in Fig. 7 is used and the time step is $\Delta t = 600$ s. The liquid fraction is taken to vary as

$$u_\ell = \min\left[1, \max\left(0, \frac{1}{2\delta}(T - T_m + \delta)\right)\right], \tag{33}$$

where a value of value of $2\delta = 2°\text{C}$ has been used. This value should be compared to the characteristic temperature interval of the problem, i.e. $T_0 - T_b = 400°\text{C}$. In Fig. 8 the front positions are shown at three different times and as can be seen the agreement between analytical and numerical solution is quite reasonable, even for the very coarse time discretization used. The number of iterations in each time step varies between 3 and 5, except in the very first step where 10 iterations are needed.

5.3 Example 3: freezing around a buried pipe

The last example deals with the problem of freezing around a pipe buried in wet soil as shown in Fig. 9. As

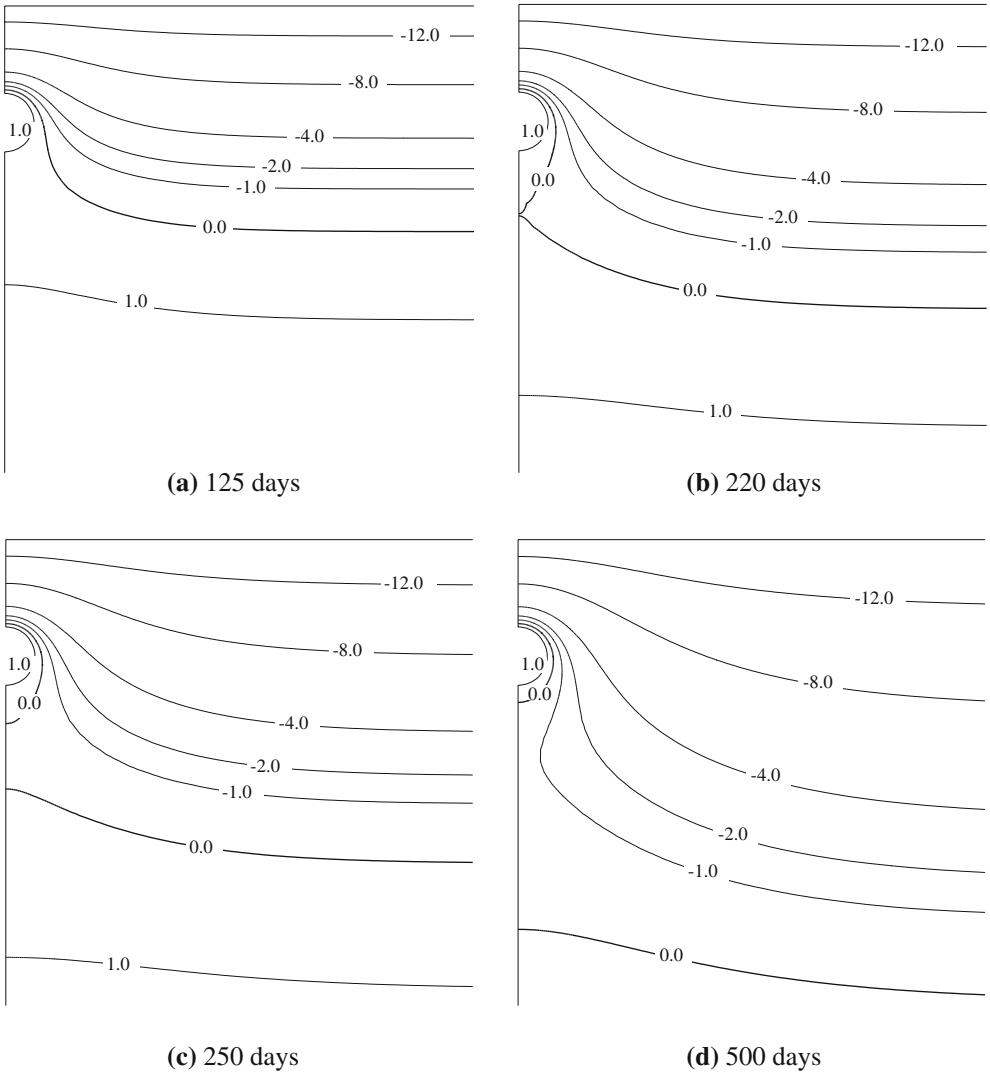

Fig. 10 Temperature distributions around buried pipe. **a** 125 days, **b** 220 days, **c**250 days and **d**500 days

already mentioned wet soil is a material whose enthalpy–temperature relation exhibits a mushy zone. The existence of a mushy zone is in part due to capillarity by which the chemical potential of the water is lowered and liquid water may exist at temperatures well below 0°C [12, 13]. For real soils also the naturally occurring salts will contribute to lowering the freezing temperature [13, 14].

Kujala [15] has experimentally examined some 68 soils and found that the volumetric unfrozen water content could be fitted by the expression

$$W = W_0 \mathrm{e}^{-(T/a)^b}, \tag{34}$$

where W_0 is the moisture content at 0°C and a and b are empirical constants which depend on the particular type of soil.

Neglecting the heat capacity of the air found in an unsaturated soil the total enthalpy–temperature relation can be written as

$$H = [\rho c_{\mathrm{w}} W + \rho c_{\mathrm{i}}(W_0 - W) + (1-n)\rho c_{\mathrm{s}}](T - T_{\mathrm{m}}) + \rho \mathscr{L} W, \tag{35}$$

where n is the porosity and subscripts w, i and s refer to liquid water, ice and soil respectively. The conductivity is taken as the volumetric mean of the three components present (again neglecting the air), i.e.

$$k = k_{\mathrm{w}} W + k_{\mathrm{i}}(W_0 - W) + (1-n)k_{\mathrm{s}}. \tag{36}$$

For the transfer of heat from the surrounding air to the soil the convection boundary condition 3 with $q = 0$ has been applied. The numerical values of the parameters used are listed in Table 3.

The results of the analysis are shown in Fig. 10 in terms of the temperature distributions at different times. It is interesting to observe how the 'front' as defined by $T = T_{\mathrm{m}}$ separates around the pipe after approximately 220 days (c). As noted by Storti et al. [5] for the case of isothermal phase-change this may cause severe difficulties for front tracking methods.

As in the previous examples the number of iterations is quite moderate. For a mesh containing 13,600 nodes a time step of D t = 2.5 days gives an average of 3.3 iterations per time step whereas using D t = 5 days results in an average of 3.7 iterations per time step.

6 Conclusions

An implicit finite element procedure capable of handling phase-change problems with a mushy zone has been described. The procedure used has proven to be quite efficient and very robust. Furthermore, the results produced by the method are generally accurate and the non-physical oscillations produced by other methods are completely avoided. In this paper only examples of two-dimensional phase-change problems have been presented. However, the extension to three-dimensional problems is straightforward, as is the extension to other two-dimensional elements than the ones used in the present paper.

References

1. Carslaw HS, Jaeger JC (1959) Conduction of heat in solids. Oxford University Press, New York
2. Crank J (1967) The mathematics of diffusion. Oxford University Press, New York
3. Voller VR, Peng S (1994) An enthalpy formulation based on an arbitrarily deforming mesh for solution of the Stefan problem. Comput Mech 14:492–502
4. Lewis RW, Morgan K, Thomas HR, Seetharamu KN (1996) The finite element method in heat transfer analysis. Wiley, New York
5. Storti M, Crivelli LA, Idelsohn SR (1988) An efficient tangent scheme for solving phase–change problems. Int J Numer Meth Eng 66:65–86
6. Storti M, Crivelli LA, Idelsohn SR (1987) Making curved interfaces straight in phase–change problems. Int J Numer Meth Eng 4:375– 392
7. Fachinotti VD, Cardona A, Huespe AE (1999) A fast convergent and accurate temperature model for phase-change heat conduction. Int J Numer Meth Eng 44:1863–1884
8. Nigro N, Fachinotti VD, Huespe AE (2000) Phasewise numerical integration of finite element method applied to solidification processes. Int J Heat Mass Transf 43:1053–1066
9. Celia MA, Bouloutas ET, Zarba RL (1990) A general mass-conservative numerical solution for the unsaturated flow equation. Water Resour Res 26:1483–1496
10. Nedjar B (2002) An enthalpy-based finite element method for nonlinear heat problems involving phase change. Comput Struct 80:9–21
11. Rathjen KA, Jiji LM (1971) Heat conduction with melting or freezing in a corner. J Heat Transf 93:101–109
12. Grant S, Sletten RS (2002) Caculating capillary pressures in frozen and ice–free soils below the melting point. Environ Geol 42:130–136
13. Watanabe K, Mizoguchi M (2002) Amount of unfrozen water in frozen porous media saturated with solution. Cold Regions Sci Technol 34:103–110
14. Banin A, Anderson DM (1974) Effects of salt concentration changes during freezing of the unfrozen water content of porous materials. Water Resour Res 10(1):24–128
15. Kujala K (1989) Unfrozen water content of Finnish measured by NMR. In: Rathmayer H (ed) International symposium on frost in geotechnical engineering. Espoo, Finland, pp 301–310